

Unified Elastoplastic–Viscoplastic Bounding Surface Model of Geosynthetics and Its Applications to Geosynthetic Reinforced Soil-Retaining Wall Analysis

Huabei Liu¹ and Hoe I. Ling, M.ASCE²

Abstract: The static and dynamic behaviors of reinforced soil structures are possibly subjected to the effects of creep or stress relaxation due to the time-dependent behavior of geosynthetic inclusions and backfill. To simulate the time-dependent monotonic and cyclic behavior of geosynthetics, an isothermal constitutive model is formulated within the framework of elastoplasticity–viscoplasticity. The concept of bounding surface plasticity is first utilized to formulate a time-independent cyclic model of geosynthetics. In order to capture the hardening stiffness of some polyester geosynthetics, an exponential bounding curve is used in simulating the primary loading. The time-independent version of the model was extended into an elastoplastic–viscoplastic model using overstress viscoplasticity with reference to available experimental data. The model was evaluated using creep, stress relaxation, monotonic, and cyclic loading test results obtained for different geosynthetics. It was then incorporated into a finite-element code and the static and dynamic behavior of a geosynthetic reinforced soil wall was analyzed. The analyzed results, with and without consideration to the time-dependent behavior of the reinforcements, were compared. It was demonstrated that although the end-of-construction behavior of the reinforced soil wall was less influenced by the time-dependent properties of geogrids, the long-term performance was considerably affected. The seismic response was also affected to some extent by the rate-dependent behavior of geogrids. The effects were more significant for short and/or large vertical spacing reinforcement layout.

DOI: 10.1061/(ASCE)0733-9399(2007)133:7(801)

CE Database subject headings: Time dependence; Geosynthetics; Viscoplasticity; Creep; Plasticity.

Introduction

Geosynthetic materials that are manufactured from polymers are commonly used to reinforce soils (Koerner 1997). The reinforced soil structures are subjected to creep or stress relaxation due to the time-dependent behavior of geosynthetic reinforcements and possibly that of the soil (Holtz et al. 1982; Wu and Helwany 1996). In seismically active regions, after experiencing sustained creep or stress relaxation, soil structures may then be subjected to earthquake loadings. The time-dependent performance of geosynthetic reinforced soil (GRS) structures is of great importance, but the issue has not been fully explored. In most design codes, only creep is explicitly accounted for, while relaxation is implicitly included via a creep reduction factor (Koerner 1997). Hence, the time-dependent deformation and stress redistribution in the geosynthetic reinforcements throughout their service life are still not clarified. At the moment, the design of GRS structures, especially if earthquake performance is an issue, does not take

into proper account the time-dependent behavior of geosynthetic reinforcements.

In order to understand the time-dependent properties of geosynthetics, experimental work has been conducted on various types of geosynthetic materials (Finnigan 1977; Allen et al. 1982; Greenwood 1990; Leshchinsky et al. 1997). Most of the experiments were conducted with respect to the creep properties of geosynthetics, with few attempts in investigating the stress relaxation behavior. A limited number of experimental studies investigating the tensile properties of geosynthetics under cyclic loading have also been attempted, examples of which included the tests by Bathurst and Cai (1994), Moraci and Montanelli (1996), Ashwamy and Bourdeau (1996), Ling et al. (1998), Kongkitkul et al. (2004).

Numerical methods have proved to be effective in investigating the sophisticated behavior of GRS structures (e.g., Ling et al. 1995; Cai and Bathurst 1995; Ling et al. 2004, 2005a). However, a proper modeling of the essential components of GRS retaining walls (RWs), including soil, geosynthetic reinforcements, and soil–geosynthetic interfaces, determines the accuracy of numerical simulations. In order to capture the time-dependent properties of geosynthetics, different constitutive models have been used (Finnigan 1977; Shrestha and Bell 1982; Andrewes et al. 1986; Findley 1987; Matichard et al. 1990; Helwany and Wu 1992; Soong and Koerner 1998; Kaliakin and Dechasakulsom 2002), most of which were creep models, with few attempts in combining creep and stress relaxation (Kaliakin and Dechasakulsom 2002). For seismic applications, only a few models were proposed that could simulate the tensile behavior of geosynthetics under cyclic loading to some extent (Cai and Bathurst 1995; Ling et al.

¹Associate Professor, Dept. of Civil Engineering, Tsinghua Univ., Beijing 100084, China.

²Associate Professor, Dept. of Civil Engineering and Engineering Mechanics, Columbia Univ., New York, NY 10027.

Note. Associate Editor: Majid T. Manzari. Discussion open until December 1, 2007. Separate discussions must be submitted for individual papers. To extend the closing date by one month, a written request must be filed with the ASCE Managing Editor. The manuscript for this paper was submitted for review and possible publication on June 14, 2005; approved on November 3, 2006. This paper is part of the *Journal of Engineering Mechanics*, Vol. 133, No. 7, July 1, 2007. ©ASCE, ISSN 0733-9399/2007/7-801-815/\$25.00.

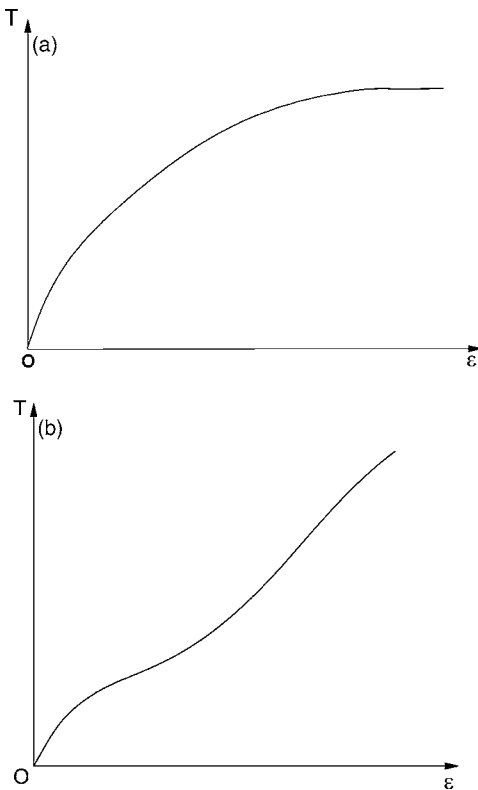


Fig. 1. Schematic sketch of nonlinear load–strain relationships of geosynthetics: (a) Type A; (b) Type B

2001). However, the simulation of GRS structures, from construction to long-term service, including seismic loading while in service, requires a constitutive model of geosynthetics that can capture the essential features of monotonic, sustained, and cyclic loadings as well as stress relaxation. Very limited studies could be found on this issue. Perkins (2000) was one of the few who developed a constitutive model for geosynthetics based on orthotropic elastoplasticity and creep formulations. However, this model was extremely complicated and the behavior under cyclic loading was not well simulated.

According to the aforementioned experimental work on geosynthetics, the salient features of the nonlinear, cyclic, and time-dependent behaviors of geosynthetics may be summarized as follows:

1. The monotonic load–strain relationship is nonlinear. Two different types of nonlinear load–strain relationship can be identified, as shown in Figs. 1(a and b). Most geosynthetic materials manufactured from polypropylene (PP) and high-density polyethylene (HDPE) exhibit nonlinear properties, as shown in Fig. 1(a), where the tangential stiffness decreases with an increase in tensile strain (hereafter known as Type A). Fig. 1(b) shows the hardening nonlinear load–strain relationship of polyester (PET) geogrids, of which the tangential stiffness first reduced with straining and then increased with an increase in the tensile strain (hereafter known as Type B).
2. Upon unloading, plastic strain accumulates in the geosynthetic specimen. The unloading and reloading cycles exhibit hysteresis. With an increase in the loading cycles, the hysteresis loops became smaller (damping is reduced)—that is, the accumulation of residual strain slows down, and the variation of stiffness with the loading cycles becomes

smaller. Fig. 2(a) shows typical cyclic loading test results of a HDPE geogrid (Ling et al. 1998).

3. The load–strain relationship of geosynthetics generally depends on the strain rate, as shown in Fig. 2(b), which is the experimental result on a HDPE geogrid by Bathurst and Cai (1994). The stiffness increases with an increase in the loading rate for PP and HDPE. Geogrids manufactured from PET are less affected by the loading rate.
4. The creep behavior of geosynthetics is dependent on the load level. Creep strain is large corresponding to the magnitude of tensile load. On the other hand, the load relaxation of geosynthetics is determined by the strain level at the instant of loading (instant strain). With an increase in the instant strain, the load relaxation becomes larger. Figs. 2(c and d) show the creep and load relaxation test results, respectively, on a geogrid specimen reported by Leshchinsky et al. (1997).
5. At the beginning of creep or load relaxation test, the creep or relaxation rate is the largest. If the load level is moderate, the creep shall finally stabilize. Some types of PP and HDPE geosynthetics exhibit a considerable amount of tertiary creep at a large load level, as shown in Fig. 2(c). However, for PET geogrids, no obvious tertiary creep exists, as reported by Leshchinsky et al. (1997). The load relaxation of geosynthetics, on the other hand, shall finally stabilize at a certain load level, depending on the instant strain level.
6. The time-dependent properties of geosynthetics are considerably influenced by temperature.

The purpose of this paper is to develop a constitutive model for geosynthetics that is relatively simple yet satisfactorily simulates aforementioned observations. The effects of temperature are not included in the proposed formulation. The proposed model, which was extended from the model proposed by Ling et al. (2001), is based on bounding surface elastoplasticity viscoplasticity. It was formulated in a hierarchical manner so that both time-independent and time-dependent behavior are simulated. Since the configuration of most geosynthetic reinforcements in GRS structures could be simplified as plane strain, a one-dimensional (1D) constitutive model is adequate for most 2D numerical analyses of GRS structures. The model was then incorporated into a finite-element code, and a modular-block GRS-RW of height 6 m was analyzed using different reinforcement layouts. The results were compared and discussed.

Proposed Geosynthetic Model

Concepts of Bounding Surface Plasticity and Overstress Viscoplasticity

Bounding surface plasticity was originally proposed by Dafalias and Popov (1975, 1976, 1977) and independently by Krieg (1975) for the simulation of the stress–strain hysteresis of metals under cyclic loading. In the 1D bounding surface plasticity, the current stress state σ is related to the image stress $\bar{\sigma}$ at the bounding lines on the stress–plastic strain ($\sigma - \epsilon_p$) plane through a mapping rule [Fig. 3(a)]. The plastic modulus E_p is expressed as a function of the distance between σ and $\bar{\sigma}$, denoted as δ , and the slope of the bounding lines, denoted as \bar{E}_p

$$E_p = \frac{d\sigma}{d\epsilon_p} = \bar{E}_p + h \frac{\delta}{\delta_{in} - \delta} \quad (1)$$

where δ_{in} = value of δ at the start of yielding along the present loading path; and h = hardening parameter. The bounding lines

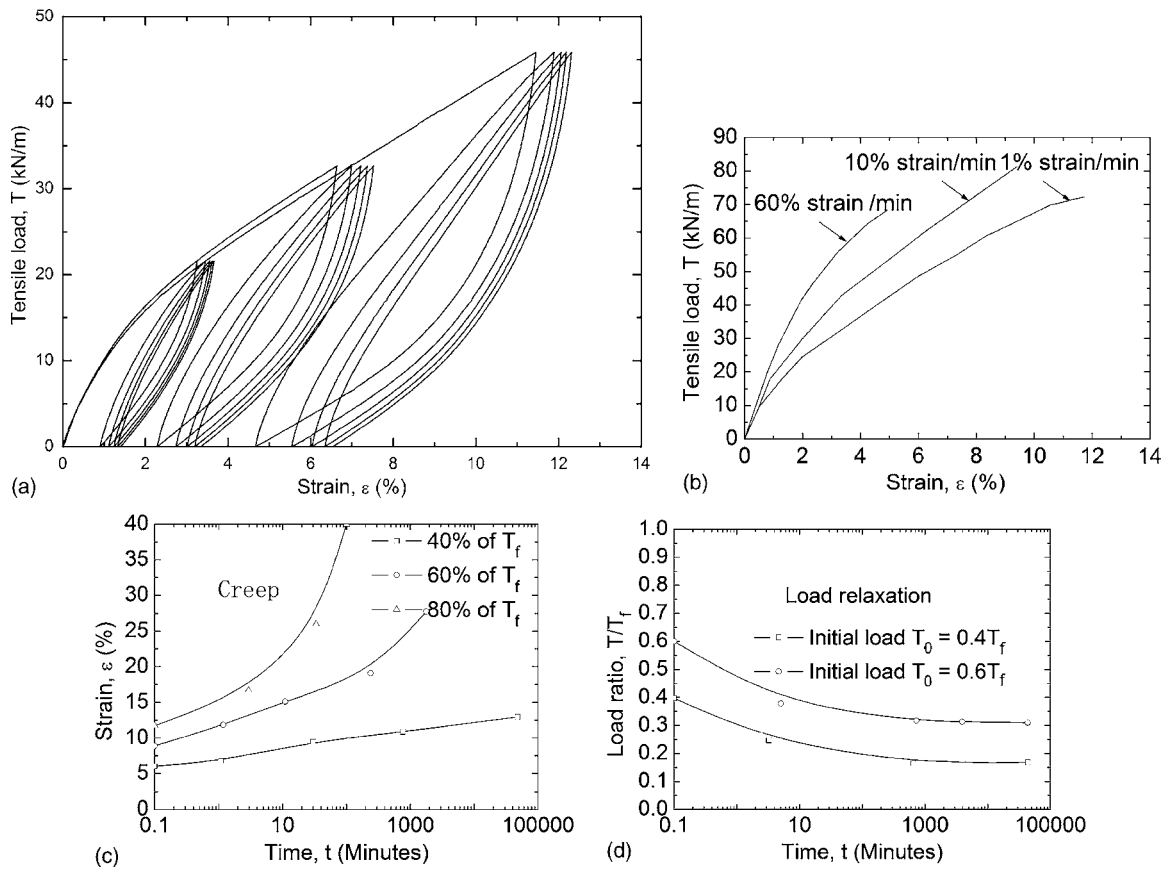


Fig. 2. Load–strain response of geosynthetics: (a) HDPE geogrid [adapted from Ling et al. (1998)]; (b) HDPE geogrid [adapted from Bathurst and Cai (1994)]; (c) creep [adapted from Leshchinsky et al. (1997)]; and (d) load relaxation [adapted from Leshchinsky et al. (1997)]

may remain straight ($\bar{E}_p = \text{constant}$) or they may vary with the hardening of the bounds. The bounding surface plasticity allows plastic strain inside the bounding surface and the smooth transition between the elastic and plastic states as well as that between unloading and reverse loading, so that the theory is very relevant for simulating cyclic behavior of materials.

Bounding surface plasticity has been used successfully to model the cyclic behavior of metal elements (Pettersson and Popov 1977; Shen et al. 1995). Ling et al. (2001) formulated a cyclic model for geosynthetic reinforcements using the bounding surface concept, and it was used in the dynamic analysis of GRS-RWs (Liu 2002; Ling et al. 2004, 2005a). A total of nine model parameters are needed to describe the cyclic behavior of geosynthetics in the original model.

Perzyna viscoplasticity has been used successfully for modeling the time-dependent behavior of materials (Gilat 1984; Kaliakin and Dafalias 1990a,b). The overstress viscoplasticity of Perzyna type (Perzyna 1966) is expressed as

$$\dot{\varepsilon}_{ij}^{vp} = \frac{1}{\eta} (\Delta\hat{\sigma})^n \frac{\partial g}{\partial \sigma_{ij}} \quad (2)$$

where $\Delta\hat{\sigma}$ = overstress; g = plastic potential function; and η = viscous coefficient. The quantity $\partial g / \partial \sigma_{ij}$ determines the direction of the viscoplastic strain rate. The 1D form of Eq. (2) may be written as

$$\dot{\varepsilon}^{vp} = \frac{1}{\eta} (\Delta\hat{\sigma})^n \text{sign}(\dot{\varepsilon}) \quad (3)$$

In 1D overstress viscoplasticity, $\Delta\hat{\sigma}$ represents the distance between the present stress state and its mapping stress, the so-called back stress, on the static curve (described subsequently).

Model Formulations

The constitutive model for geosynthetics (Types A and B) was formulated in a hierarchical manner, allowing it to be used in different applications, considering both time-dependent and time-independent behavior. The proposed constitutive equations are regarded as a single model because they share the same structure and model parameters, and hence only one main subroutine is needed for the finite-element implementation.

A bounding surface model is first developed and then extended to include the rate effects. It is assumed that the geosynthetic reinforcement does not sustain compression and temperature effects are not considered.

The time-independent version of the model was modified from Ling et al. (2001) by considering nonlinear bounding lines. In the model, the total tensile strain increment $d\varepsilon$ is assumed to consist of the elastic $d\varepsilon^e$ and plastic $d\varepsilon^p$ components

$$d\varepsilon = d\varepsilon^e + d\varepsilon^p \quad (4)$$

It is assumed that no real elastic behavior exists in the present model—that is, plastic strain develops at the very beginning of

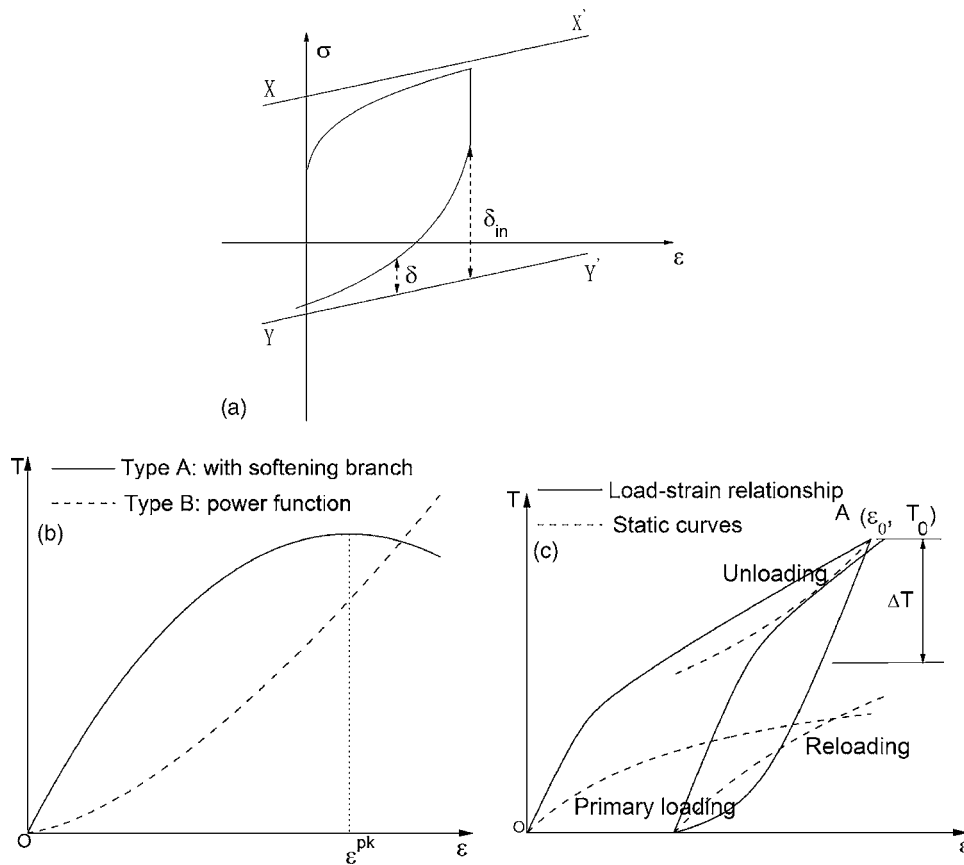


Fig. 3. Bounding surface concept and static curves: (a) conceptual sketch of bounding surface model [adapted from Ling et al. (2001)]; (b) conceptual sketch of static curve; and (c) kinematical static curves during unloading and reloading

loading and unloading. The assumption is based on the fact that most geosynthetics exhibit inelastic and nonlinear behavior even at very low load level, and upon unloading, the range of pure elastic response is very small and negligible for practical purposes (Cai and Bathurst 1994; Ling et al. 1998). The assumption is also made for the sake of simplicity, since no parameter on the elastic limit (or yield load level) would be required in the model. The time-independent response of geosynthetics is thus assumed to be elastoplastic (elastoplastic viscoplastic for the time-dependent response) at all load levels. A similar assumption was used in the modeling of soil behavior (Pastor et al. 1990; Ling and Liu 2003).

The load per unit width T , instead of stress σ , is used for geosynthetics which are planar members. For Type A geosynthetics, the bounding lines on the load–plastic strain (T – ε^p) plane are both represented by straight lines. The bounding line on the compression side is used only to express the unloading behavior, as the model does not sustain compression. In the model by Ling et al. (2001), the two bounding lines on the tension and compression sides are not parallel, whereas in the proposed model, they are simplified to be parallel. Thus, the bounding lines on the tension and compression sides of the T – ε^p plane are defined as

$$T_+ = A + \bar{J}_p \varepsilon^p; \quad T_- = B + \bar{J}_p \varepsilon^p \quad (5)$$

where A and B =intercepts of the bounding lines with the load axis (T axis); \bar{J}_p =slope of the bounding lines; and T_+ and T_- =bounding loads per unit width on the tension and compression sides, respectively.

For Type B geosynthetics, the bounding lines are more complicated. The bounding line for primary loading is different from that of unloading and reloading. By observing the behavior of Type B geosynthetics, the bounding line for primary loading is defined using an exponential function

$$T_+^V = A + \exp(C\varepsilon^p) - 1 \quad (6)$$

where C =model parameter. Therefore, the slope of the bounding line for primary loading is

$$\bar{J}_p^V = C \exp(C\varepsilon^p) \quad (7)$$

The bounding lines for unloading and reloading are parallel to each other, similar to the bounding lines for Type A geosynthetics

$$T_+^R = A_R + C\varepsilon^p; \quad T_- = B + C\varepsilon^p \quad (8)$$

where A_R =intercept of the reloading bounding line with T axis. The initial slope of Eq. (6) is the same as the slopes of Eq. (8). That is, the slopes for unloading and reloading are

$$\bar{J}_p^U = \bar{J}_p^R = C \quad (9)$$

As emphasized by Ling et al. (2001), a single hardening parameter h is not adequate in describing the cyclic behavior of geosynthetics. The cyclic experimental results on geogrids showed that the hardening during reloading is controlled by the plastic strain, while the hardening during primary loading can be expressed by a single hardening parameter. Therefore, in the proposed model, a power function of the plastic strain ε^p is used to express the hardening during reloading, while only one constant

Table 1. Model Parameters for Different Geosynthetics

| Parameters | Type A geosynthetics | | | Type B geosynthetics | |
|----------------------------------|-----------------------------|-----------------------------|--------------------------|------------------------------|------------------------------|
| | HDPE Geogrid 1 ^a | HDPE Geogrid 2 ^b | Geomembrane ^c | PET Geogrid 1 ⁽¹⁾ | PET Geogrid 2 ⁽²⁾ |
| J_e (kN·m) | 1,300 | 2,150 | 1,500 | 600 | 2,500 |
| A (kN·m) | 240 | 350 | 17 | 25 | 35 |
| \bar{J}_p (kN·m) | 40 | 90 | 20 | — | — |
| h_0^L (kN·m) | 200 | 600 | 500 | 140 | 700 |
| B (kN·m) | -45 | -330 | — | -30 | -200 |
| h_k^L (kN·m) | 180 | 1,300 | — | 130 | 300 |
| h_0^U (kN·m) | 1,500 | 3,000 | — | 550 | 700 |
| A_R (kN·m) | — | — | — | 70 | 180 |
| C ln(kN·m) | — | — | — | 70 | 60 |
| η (kN·m) ^{1/m} min | 2.2e9 | 2.0e9 | 2.0e6 | 1.0e9 | 5.0e9 |
| n_0 | 3.8 | 2.6 | 2.8 | 4.0 | 2.9 |
| κ | 14 | 10 | 4 | 14 | 18 |
| a_s (kN·m) | 600 | 240 | 2,400 | — | — |
| b_s (kN·m) | 710 | 326 | 2,482.8 | 606 | 9,000 |
| c_s | 1.22 | 1.909 | 1.0365 | 1.493 | 2.5 |

^aLeshchinsky et al. (1997) and Ling et al. (1998).

^bCai and Bathurst (1995).

^cMerry and Bray (1997).

hardening parameter is used for the primary loading or unloading, but of different values. The hardening parameters are expressed as

$$h^{VL} = h_0^L; \quad h^{RL} = h_0^L + h_k^L \sqrt{\varepsilon^p}; \quad h^U = h_0^U \quad (10)$$

where h_0^L , h_k^L , and h_0^U =model parameters; and superscripts L , U , and RL indicate loading, unloading, and reloading, respectively.

With the definitions of the bounding lines and the hardening parameters, the plastic stiffness of the model is obtained as

$$J_p = \frac{dT}{d\varepsilon^p} = \bar{J}_p + h \frac{\delta}{\delta_{in} - \delta} \quad (11)$$

where \bar{J}_p can be obtained using Eq. (5), (7), or (9) for different types of geosynthetics and different loading conditions, and the hardening parameter h assumes different expressions for primary loading, reloading, or unloading, as denoted in Eq. (10). Referring to Eq. (4), the total stiffness that relates load and strain of the geosynthetics is written as

$$J_T = \frac{J_p J_e}{J_p + J_e} \quad (12)$$

where J_e =elastic stiffness.

In the time-dependent version of the model, the total strain rate is assumed to be composed of the following three components:

$$\dot{\varepsilon} = \dot{\varepsilon}^e + \dot{\varepsilon}^p + \dot{\varepsilon}^{vp} \quad (13)$$

where $\dot{\varepsilon}^e$, $\dot{\varepsilon}^p$, and $\dot{\varepsilon}^{vp}$ =elastic, plastic, and viscoplastic strain rates, respectively. As the elastic and plastic loadings are rate independent, they are related to the strain increments as denoted in Eq. (4) through the following relations:

$$d\varepsilon^e = \dot{\varepsilon}^e dt; \quad d\varepsilon^p = \dot{\varepsilon}^p dt \quad (14)$$

where dt =time step.

An elastoplastic–viscoplastic formulation may be considered uncoupled (Lubliner 1972) or coupled (Kaliakin and Dafalias 1990a) from a modeling viewpoint. Theoretically, the coupled formulation may be more rational, but the uncoupled one is usu-

ally simpler and adequate for many practical problems. According to Lubliner (1972), the uncoupled formulation of elastoplasticity viscoplasticity is also thermodynamically sound. With this argument, elastoplastic response is assumed to be uncoupled with the viscoplastic response in the proposed model. It is also observed that uncoupled formulations were used in 1D modeling of other materials (Tanimoto et al. 1993).

The elastoplastic behavior of the elastoplastic–viscoplastic model can now be described by Eqs. (5)–(12) within the framework of bounding surface plasticity. However, the bounding lines in the elastoplastic–viscoplastic model must then be calibrated using the load–strain behavior of geosynthetics at very high straining rate, as discussed in subsequent sections.

The viscoplastic behavior is described using the Perzyna formulation. Several issues need to be addressed before the final relationship can be formulated. First of all, a domain that defines the boundary of the viscoplastic behavior should be obtained. The boundary is usually referred to as the *static curve*. According to the load-relaxation experimental results, the load relaxation eventually stabilizes at certain load levels, depending on the amplitude of the instant straining. In the proposed model, for Type A geosynthetics, this domain is expressed using the following function:

$$T_s = a_s \varepsilon - b_s \varepsilon^{c_s} \quad (15)$$

where a_s , b_s , and c_s =material constants. Eq. (15) is illustrated as a nonlinear curve with a softening branch [Fig. 3(b)]. The softening branch ensures that tertiary creep can be simulated when the strain level attains a large value. For Type B geosynthetics, a simple static curve was used through a power function

$$T_s = b_s \varepsilon^{c_s} \quad (16)$$

The physical meaning of Eq. (15) or (16) may be interpreted in two ways. First, at certain instant strain (ε), the load level shall finally reduce to T_s in a load relaxation test. Eqs. (15) and (16) can also be regarded as the load–strain relationship of geosynthetics at extremely low loading rate.

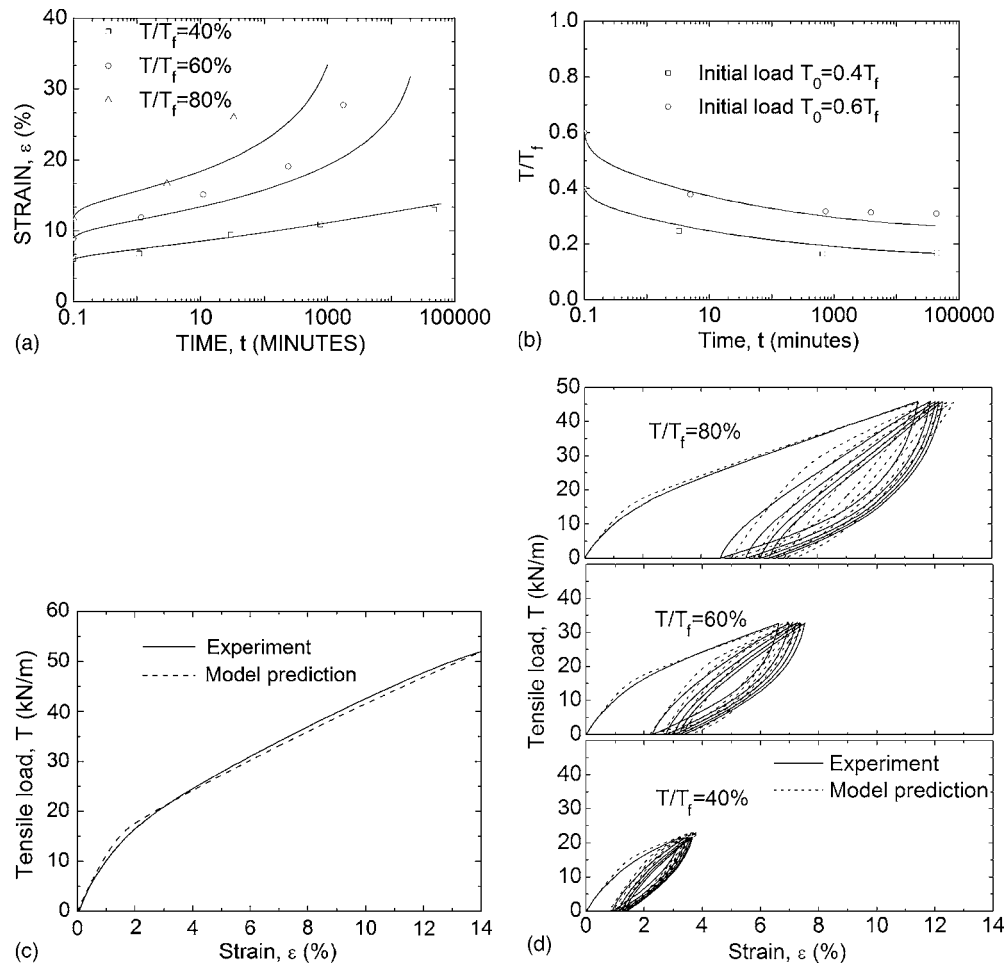


Fig. 4. Experimental results on a HDPE geogrid [adapted from Leshchinsky et al. (1997) and Ling et al. (1998)]

With the definition of Eq. (15) or (16), the viscoplastic strain rate is defined for primary loading and sustained loading as

$$\dot{\varepsilon}^{vp} = \frac{1}{\eta} |T - T_s|^n \text{sign}(\dot{\varepsilon}), \quad T \geq T_s \quad (17)$$

As defined earlier, η = viscous coefficient. The parameter n is not a constant in the proposed model. Instead, it is assumed to reduce with the increase in the viscoplastic strain ε^{vp} through an exponential function

$$n = n_0 [1 + \exp(-\kappa \varepsilon^{vp})] \quad (18)$$

where n_0 and κ = material constants.

A challenging issue is to determine the *static curves* in unloading and reloading. From the available cyclic experimental results on geosynthetics (Cai and Bathurst 1994; Ling et al. 1998), at the start of unloading or reloading the stiffness is large, indicating small amplitude of plastic and viscoplastic strain rate. The stiffness decreases as the absolute relative load $|\Delta T|$ increases, as illustrated in Fig. 3(c), which implies that the amplitudes of the plastic strain and the viscoplastic strain rates increase. The variation of plastic strain rate in unloading and reloading may be addressed by the bounding surface plasticity, while that of the viscoplastic strain rate is related to the static curves in unloading and reloading. In order to describe the aforementioned viscoplastic behavior during unloading and reloading, kinematical static curves are proposed in the model. That is, the static curve starts from the beginning of unloading or reloading and is issued in the

direction of unloading or reloading [Fig. 3(c)]. The formulations of static curves in unloading and reloading are consistent with the assumption in the primary loading.

For Type A geosynthetics, the Masing rule is employed with Eq. (15) as the backbone curve and the static curve in unloading is expressed as

$$T_s = T_0 + a_s(\varepsilon - \varepsilon_0) + 2b_s[|\varepsilon - \varepsilon_0|/2]^{c_s} \quad (19a)$$

and that in reloading is defined as

$$T_s = T_0 + a_s(\varepsilon - \varepsilon_0) - 2b_s[(\varepsilon - \varepsilon_0)/2]^{c_s} \quad (19b)$$

For Type B geosynthetics, the static curve in unloading is

$$T_s = T_0 + b_s \varepsilon^{c_s} - b_s \varepsilon_0^{c_s} \quad (20a)$$

and in reloading, it is expressed as

$$T_s = T_0 + b_s(\varepsilon - \varepsilon_0)^{c_s} \quad (20b)$$

The reference strain ε_0 in Eqs. (19) and (20) is the strain of geosynthetics at the start of unloading or reloading. The exponent n as shown in Eq. (17) is also different for unloading. It is set to be a constant during unloading

$$n^U = n(\varepsilon_0^{vp}) \quad (21)$$

in which ε_0^{vp} denotes the viscoplastic strain at the start of unloading.

The use of Eqs. (19) and (20) as the static curves in unloading and reloading leads to clarification of an additional issue. The

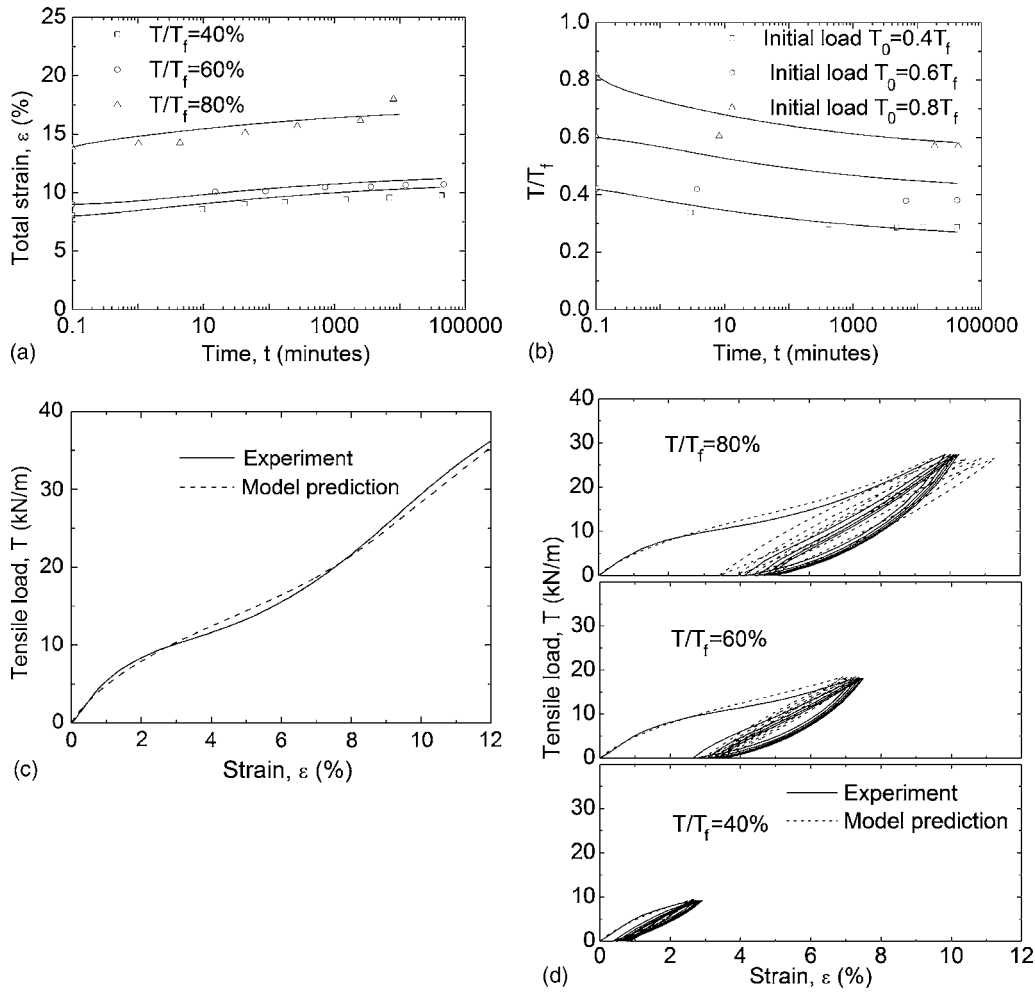


Fig. 5. Comparison between model simulations and experimental results on a PET geogrid [adapted from Leshchinsky et al. (1997) and Ling et al. (1998)]

creep or load relaxation that has taken place after unloading shall be incorrect if Eq. (19a) or (20a) is used as the reference static curve during creep or load relaxation. In the proposed model, the creep or load relaxation that has taken place after unloading and reloading utilizes the original static curve as denoted in Eq. (15) or (16). During a specific time step dt , if $|d\varepsilon^{vp}| \geq |d\varepsilon|$, then the static curve, as denoted in Eq. (15) or (16), would be used instead, no matter if it is in primary loading, unloading, or reloading. That is to say, when $|d\varepsilon^{vp}| = |d\varepsilon|$, indicating creep, or $|d\varepsilon^{vp}| > |d\varepsilon|$, implying load relaxation, Eq. (15) or (16) would be used to calculate the overstress $T - T_s$. In the proposed model, the handling of creep or load relaxation after unloading or reloading has occurred, still needs to be verified by experiments.

A tangential viscoplastic stiffness can now be defined for a time step dt as

$$J_{vp} = \frac{dT}{d\varepsilon^{vp}} = \frac{\dot{T}dt}{\dot{\varepsilon}^{vp}dt} = \frac{\dot{T}}{\dot{\varepsilon}^{vp}} \quad (22)$$

Hence, utilizing Eq. (13), the total stiffness is obtained as

$$J_T = \frac{J_{vp}J_pJ_e}{J_pJ_e + J_eJ_{vp} + J_pJ_{vp}} \quad (23)$$

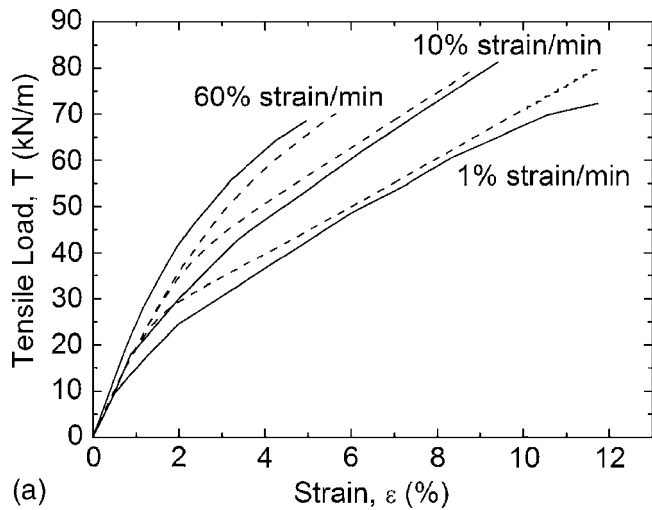
since from Eq. (13), it can be shown that

$$\frac{1}{J_T} = \frac{1}{J_e} + \frac{1}{J_p} + \frac{1}{J_{vp}} \quad (24)$$

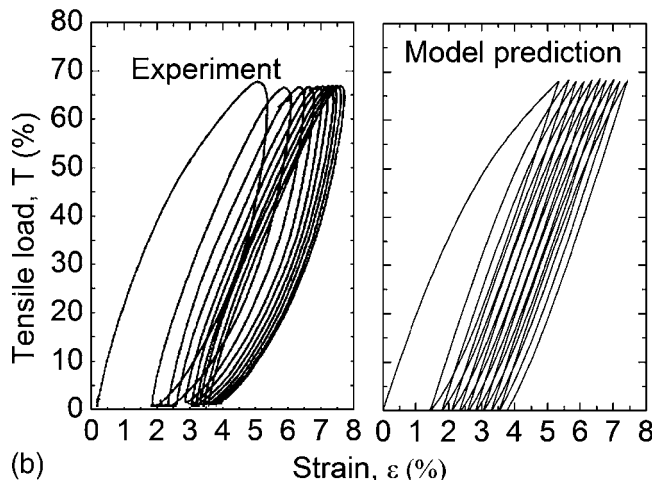
Eqs. (13) and (24) imply that the total response of geosynthetics is determined by an elastic, a plastic, and a viscoplastic element added in sequence. It must be noted that no elastic limit is included in the elements that determine the development of the plastic strain or the viscoplastic strain. Eqs. (13) and (24) also indicate that the plastic element would undergo *unloading* in relaxation, in which the total strain is kept constant and the load level decreases. Within the framework of bounding surface plasticity, plastic strain still develops during unloading. For the proposed model in which only tension is possible, the direction of plastic strain rate $\dot{\varepsilon}^p$ is opposite to that of $\dot{\varepsilon}^{vp}$ in relaxation and is negative.

Model Calibration

The time-independent model requires seven parameters for Type A geosynthetics and eight for Type B geosynthetics. There are additional six parameters for Type A geosynthetics and five for Type B if time-dependent properties are considered. Among the 13 parameters, the parameters J_e , A , B , h_0^L , h_0^U , h_k^L , η , b_s , c_s , n_0 ,



(a)



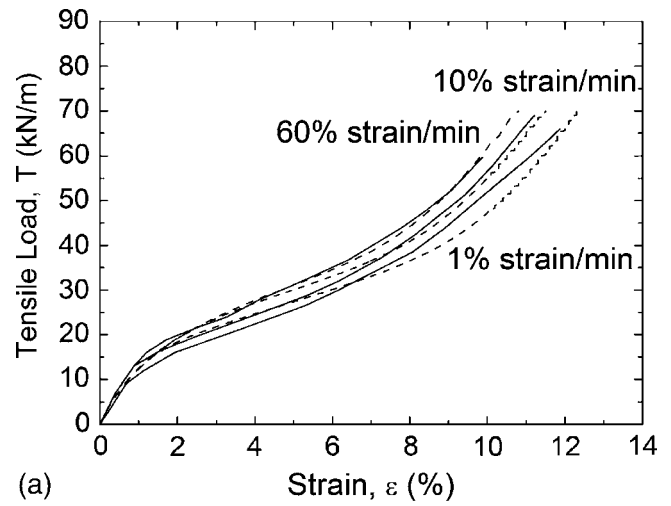
(b)

Fig. 6. Comparison between model simulations and experimental results on a HDPE geogrid [adapted from Bathurst and Cai (1994)]

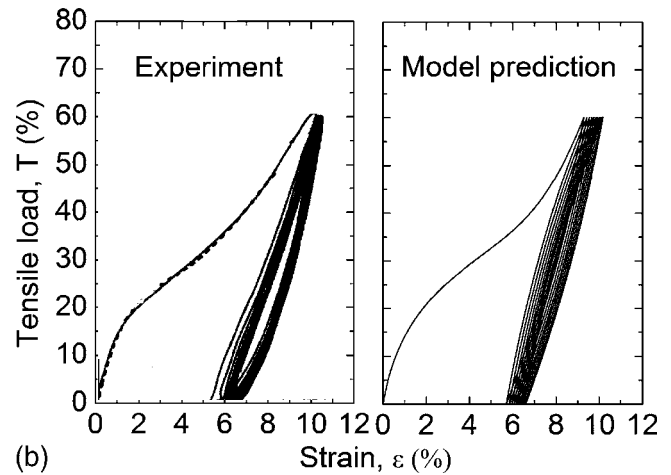
and κ are shared by the two types of geosynthetics, while Type A geosynthetic requires two additional parameters, \bar{J}_p and a_s , and Type B needs A_R and C .

The calibration of model parameters for the time-independent version of the model is reported elsewhere (Liu and Ling 2006) and will not be repeated. The calibration of the time-dependent model is described as follows. A monotonic test at sufficiently large loading rate, a creep or load relaxation test with sufficiently large initial load level, and a cyclic test (preferably at different magnitudes) are necessary to calibrate all the model parameters. For Type A geosynthetics, a creep test at large load level would be required to calibrate the parameter for tertiary creep. As the elastoplastic and viscoplastic behavior of the proposed model are assumed to be uncoupled, a monotonic test at sufficiently large loading rate (such as 50% strain per minute) is preferable in calibrating the model parameters for the bounding lines. However, model parameters with acceptable accuracy could still be obtained as discussed subsequently if only low loading-rate test results are available.

The viscous parameters (a_s , b_s , c_s , η , n_0 , and κ) are first calibrated using the creep or load relaxation experimental results. If load relaxation experimental results are available, for Type B geosynthetics, b_s and c_s are obtained by matching the stabilizing loads in the relaxation tests; for Type A geosynthetics, the



(a)

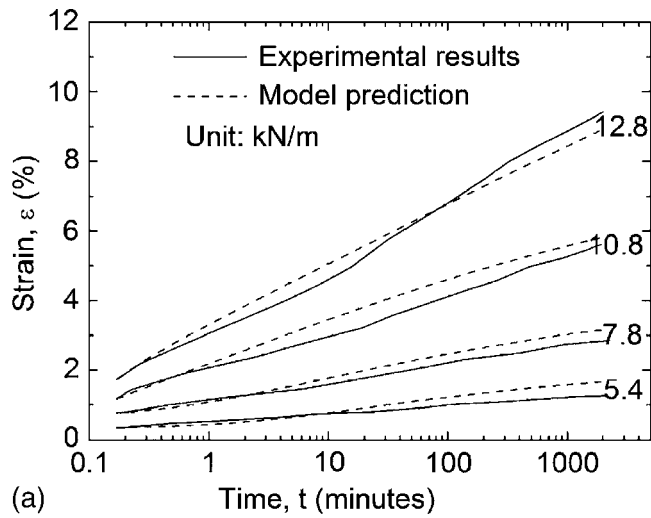


(b)

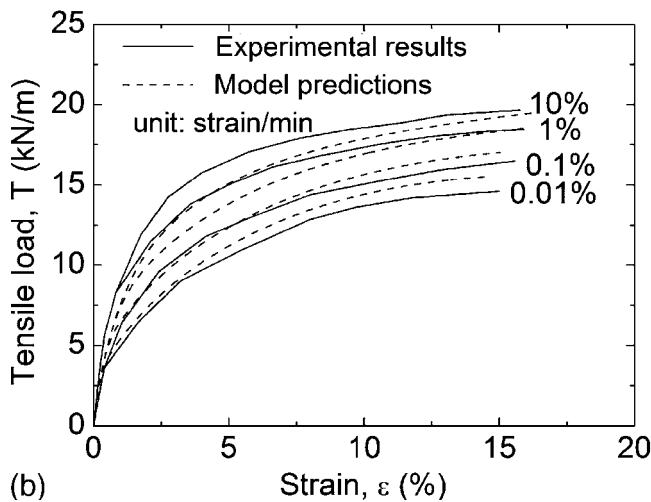
Fig. 7. Comparison between model simulations and experimental results on a PET geogrid [adapted from Bathurst and Cai (1994)]

strain level at which tertiary creep occurs is the peak strain ϵ^{pk} [Fig. 3(b)], and together with the stabilizing loads in the load relaxation tests, the parameters a_s , b_s , and c_s can be calibrated. However, if load relaxation tests are not conducted, the viscous parameters can also be obtained by simply calibrating against creep experimental results. Since in the proposed model, $\dot{\epsilon}^c = \dot{\epsilon}^p = 0$ during creep tests, we have $\dot{\epsilon} = \dot{\epsilon}^{vp}$. With the creep curves, ϵ^{vp} and ϵ^{vp} at different time intervals can be obtained. The viscous parameters can then be calibrated by solving Eqs. (17) and (18), since the load level T is known, and the viscoplastic strain rates $\dot{\epsilon}^{vp}$ and strains ϵ^{vp} at several time intervals are also known.

The elastic parameter J_e is then taken as the initial slope of the monotonic load-strain curve. The slope of the bounding lines \bar{J}_p for Type A geosynthetics and the parameter C for Type B are obtained using the slope of the monotonic curve with sufficiently large loading rate at large strain. For Type B geosynthetics, Eq. (7) can be used to calibrate the parameter C . The other monotonic parameters h_o^L and A are calibrated by matching the monotonic load-strain curve. If a large-loading rate test is not available, the parameter A could be given a sufficiently large value (larger than or equal to the rupture strength in the loading test). The other parameters can then be obtained by matching the monotonic load-strain curve. However, the behavior of the model at different loading rates must be checked to ensure that



(a)



(b)

Fig. 8. Comparison between model predictions and experimental results on a HDPE geomembrane [adapted from Merry and Bray (1997)]

the stiffness at very large loading rate should be sufficiently large compared to the one at low loading rates.

The unloading parameters (B and h_0^U) are then calibrated using the unloading behavior of geosynthetics, preferably at various loading amplitudes. The reloading parameters h_k^r and A_R for Type B geosynthetics are finally calibrated using the reloading behavior.

It may be worthwhile to point out that the time-independent version of the model can be obtained using the time-dependent one by setting the parameter η to a very large value. Therefore, only one computer code is needed for both the time-independent and time-dependent versions of the model.

Model Evaluation

The capability of the model in simulating the monotonic, cyclic, creep, and load relaxation behavior of geosynthetics was evaluated using the experimental results of Leshchinsky et al. (1997), Ling et al. (1998), and Bathurst and Cai (1994). The HDPE geogrid (C2) and PET geogrid (A1) in Leshchinsky et al. (1997) are the same as the geogrids C and B in Ling et al. (1998), respec-

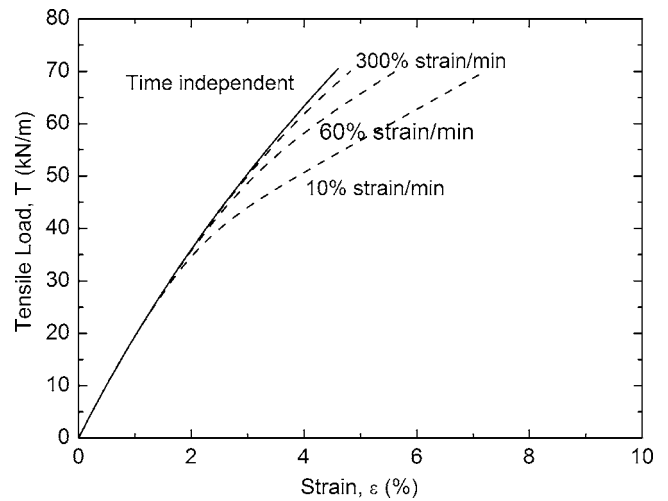


Fig. 9. "Saturation" behavior of the time-dependent model

tively. Hence, the creep and stress relaxation experimental results of Leshchinsky et al. (1997) were used to calibrate the time-dependent parameters of the model, while the monotonic and cyclic parameters were calibrated using the results of Ling et al. (1998). The monotonic and creep behavior of a HDPE geomembrane were also simulated using the experimental results of Merry and Bray (1997).

The time-independent version of the model has been evaluated and reported elsewhere (Liu and Ling 2006) due to length restrictions. The model was able to predict the monotonic and cyclic behavior of different geogrids with acceptable accuracy.

Two geogrids were simulated using the time-dependent version of the model, based on the experimental results of Leshchinsky et al. (1997) and Ling et al. (1998). The procedures as described in the previous section are used to calibrate the model. As the loading rates in Ling et al. (1998) was 10% strain per minute, the alternative procedure for calibrating the monotonic model parameters as discussed was used. The model parameters for these two geogrids are summarized in Table 1.

The results of simulations of the creep and load relaxation behavior of the HDPE geogrid are shown in Figs. 4(a and b), respectively. It is seen that the model simulates the creep and load relaxation behavior to an acceptable extent. Attention is focused on the modeling of tertiary creep when the applied load is large. The simulations of the monotonic and cyclic behavior are shown in Figs. 4(c and d). The hysteresis, residual strain accumulation, and stiffness variation during cyclic loading are all described by the model. Figs. 5(a–d) show the comparison between the model

Table 2. Model Parameters for Backfill and Foundation Soils

| Parameters | Values | Parameters | Values |
|------------------------|--------|----------------|---------|
| ϕ_{p0} (degrees) | 39.4 | β_0 | 20 |
| $\Delta\phi$ (degrees) | 0.5 | α | 0.47 |
| M_g | 1.4 | H_0 (kPa) | 50,000 |
| M_f | 0.645 | H_{u0} (kPa) | 100,000 |
| G_0 (kPa) | 50,000 | r | 5 |
| K_0 (kPa) | 55,000 | r_u | 0 |
| k_s | 0.1 | r_d | 400 |
| β_{10} | 3.1 | | |

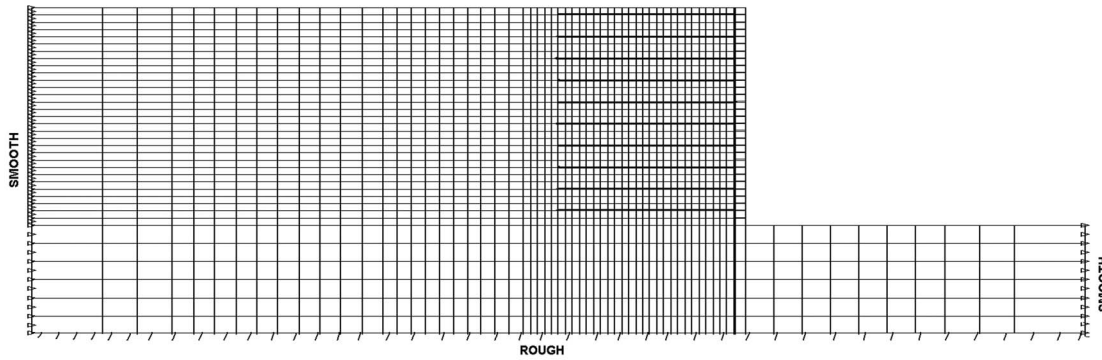


Fig. 10. Finite-element mesh

simulations and experimental results of the PET geogrid. The creep and load relaxation of the PET geogrid were small compared to those of the HDPE geogrid and the model simulated both of them satisfactorily. The simulations of the monotonic and cyclic load-strain relationships were also good.

The monotonic tests at various loading rates and the cyclic tests on a HDPE geogrid and a PET geogrid of Cai and Bathurst (1995) were also simulated using the proposed model. These two geogrids were not the same as those in Leshchinsky et al. (1997) and Ling et al. (1998). As no creep or load relaxa-

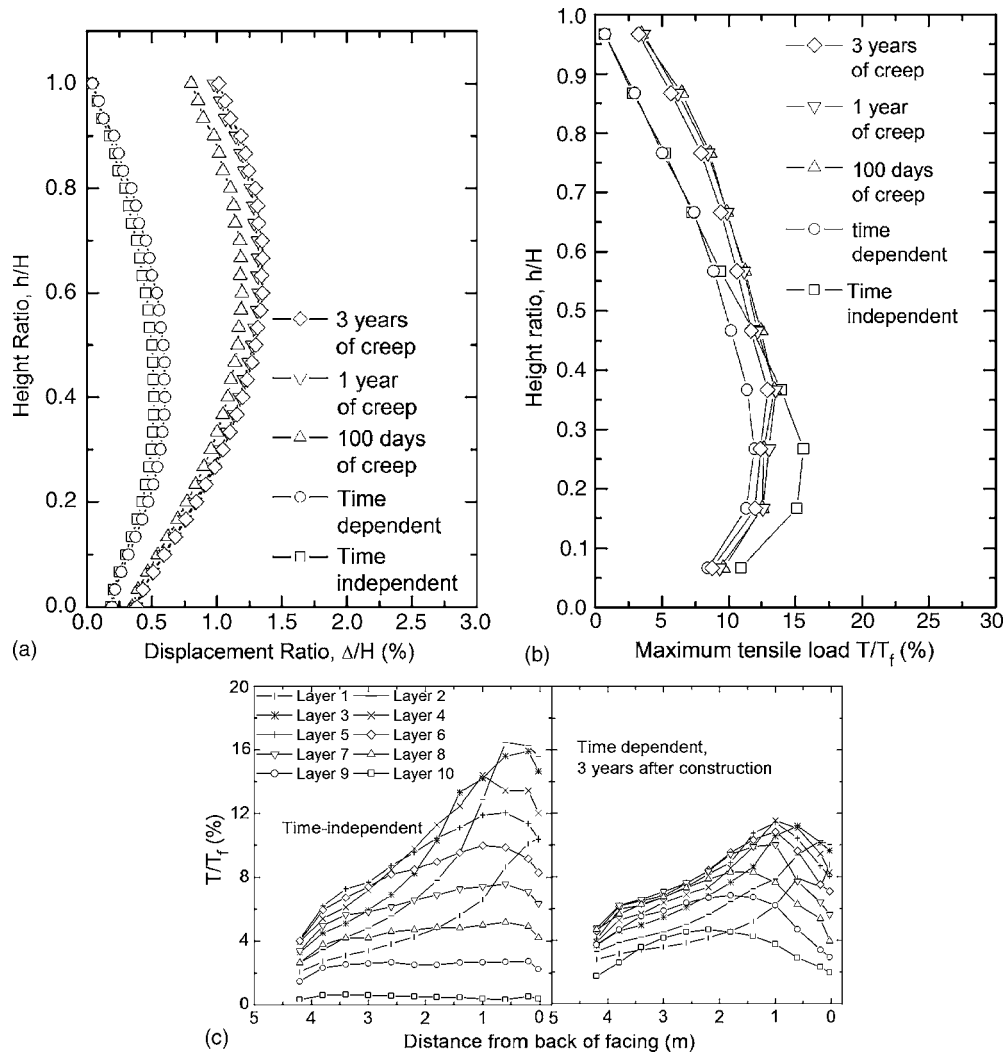


Fig. 11. Performance of GRS-RW at end of construction and different periods of creep with regular reinforcements: (a) lateral displacement; (b) maximum load in the reinforcement layers; and (c) load distribution along the reinforcement layers

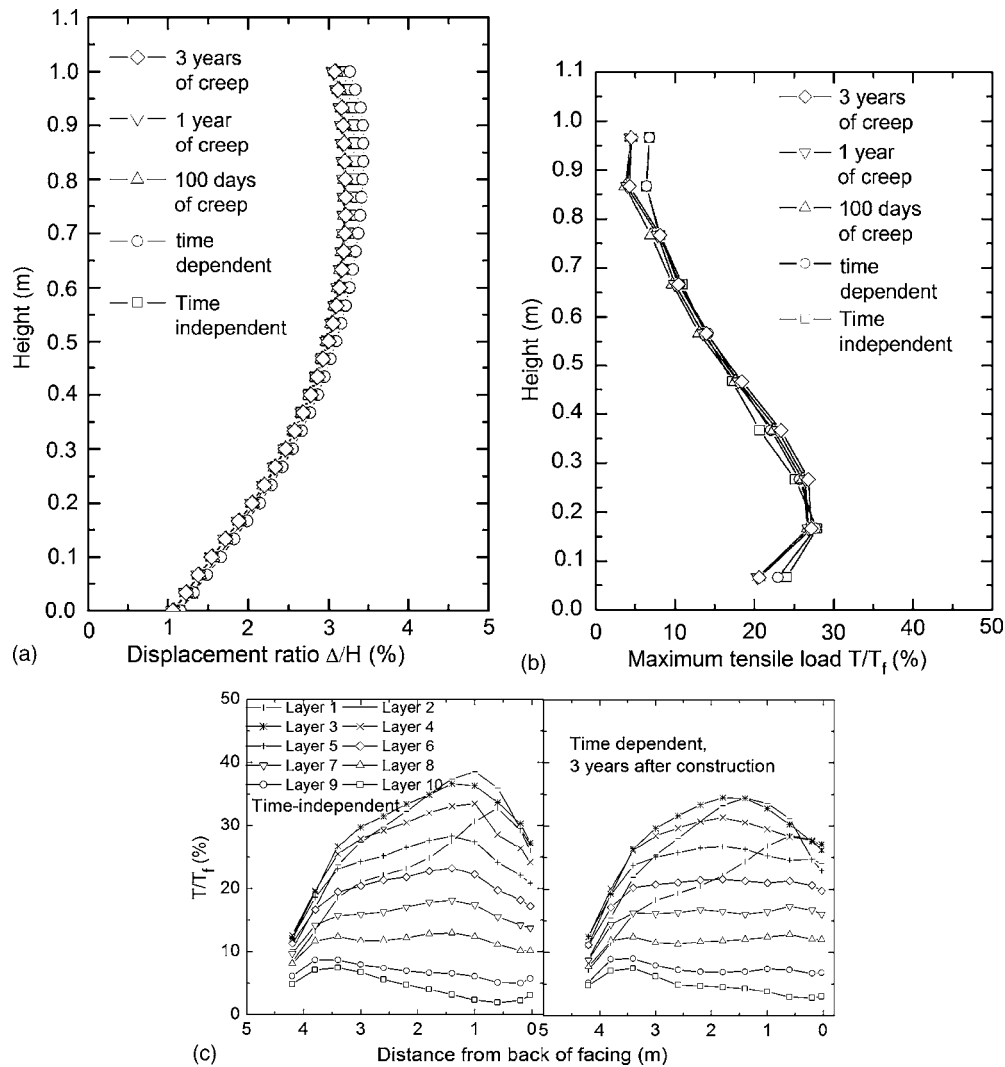


Fig. 12. Seismic performance of GRS-RW with regular reinforcements: (a) lateral deformation of facing induced by earthquake; (b) maximum reinforcement loads induced by earthquake; and (c) earthquake-induced load distribution in the reinforcements

tion experimental results were reported, the viscous parameters (a_s , b_s , c_s , η , n_0 , and κ) were obtained together with the monotonic parameters (J_e , \bar{J}_p , C , h_o^L , and A) using the monotonic load-strain relationships at various loading rates [Figs. 6(a) and 7(a)]. The model simulations and experimental results of the cyclic tests are compared in Figs. 6(b) and 7(b). The capability of the model in simulating the load-strain relationships at different loading rates in a certain range was demonstrated.

The simulations of the creep and rate effects on monotonic tests of a HDPE geomembrane of Merry and Bray (1997) are shown in Fig. 8. The viscous model parameters (a_s , b_s , c_s , η , n_0 , and κ), were obtained using the creep experimental results, and the monotonic parameters (J_e , \bar{J}_p , C , h_o^L , and A) were calibrated using the monotonic loading test result with a loading rate of 10% strain per minute. It can be seen that the accuracy of simulations of the model is acceptable.

The issue of strain rate effects in the proposed model deserves further discussion. As can be seen in the simulations of the experimental results of Cai and Bathurst (1995) and Merry and Bray (1997), the model is able to capture the strain rate effects to a certain extent. However, the proposed model exhibits the problem of strain-rate "saturation" associated with time-dependent bound-

ing surface formulation as discussed in Kaliakin and Dafalias (1990a,b). With very large loading rate, the model will predict time-independent response. The model parameters calibrated from the experimental results in Cai and Bathurst (1995) were used to investigate the model behavior at very large strain rate. It can be seen from Fig. 9 that at very large strain rate (using 300% strain per minute), the load-strain relationship as predicted by the proposed model is very close to the time-independent one. Nevertheless, the loading rates in geosynthetic reinforcements in most applications would usually be in a range that can be described by the proposed model, say less than 100% per minute, as demonstrated in Figs. 6-8.

Applications to Reinforced Soil Retaining Wall Analysis

The proposed geosynthetic model was incorporated into a modified version of the finite-element (FE) code DYNA SWANDYNE-II (Chan 1993; Liu 2002). The capacity of this FE program in analyzing the static and dynamic behavior of GRS-RWs has been demonstrated in Ling et al. (2004, 2005a). In order

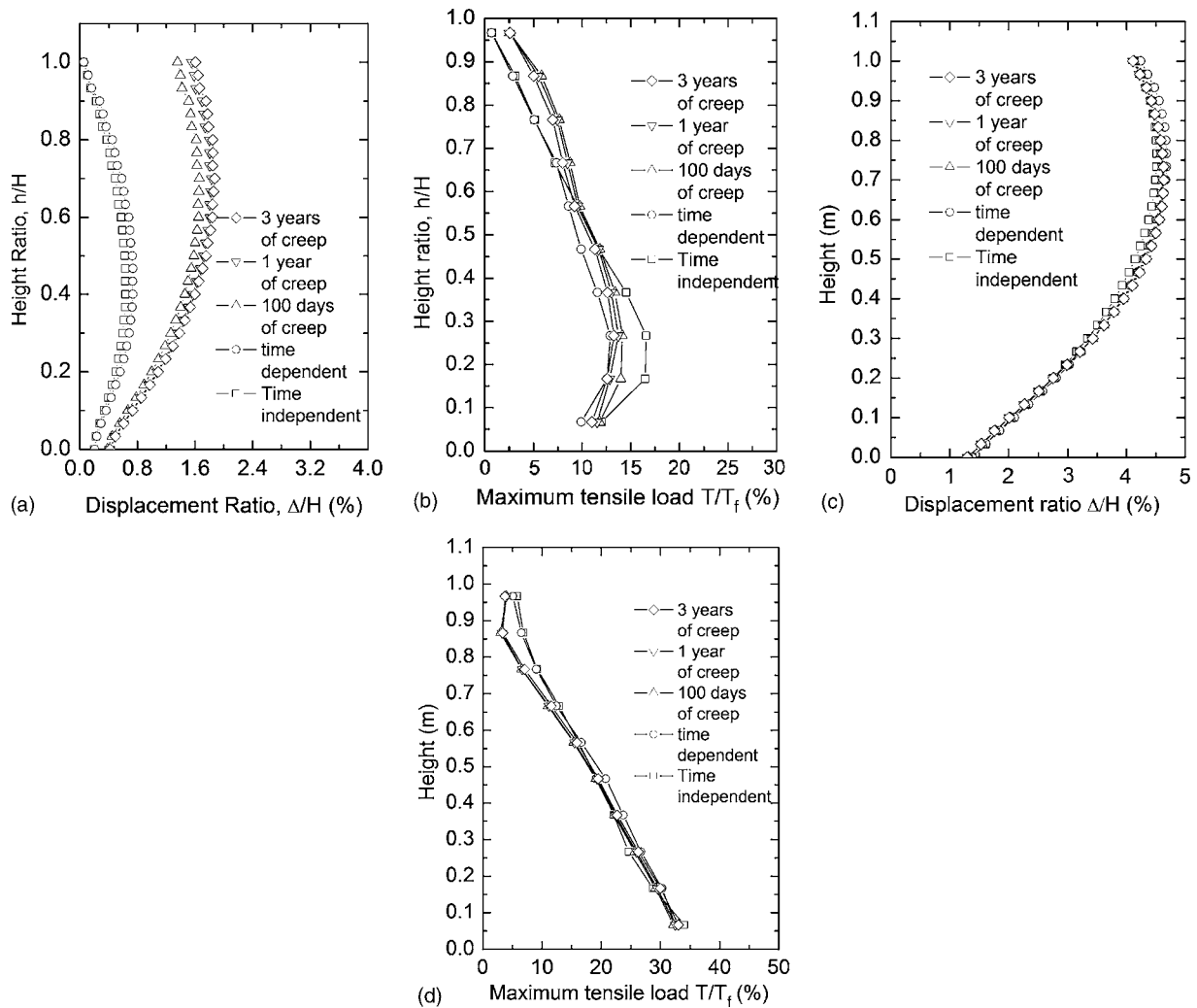


Fig. 13. Static and seismic performance of GRS-RW with short reinforcements: (a) lateral displacement; (b) maximum load in the reinforcement layers; (c) lateral deformation of facing induced by earthquake; and (d) maximum reinforcement loads induced by earthquake

to investigate the effects of time-dependent behavior of geosynthetics in the wall performance, a 6-m-high modular-block GRS-RW was analyzed. Both the time-independent and time-dependent versions of the model were used to simulate the geosynthetic reinforcements.

The model wall has already been analyzed in Ling et al. (2005b) in studying the effects of design parameters on the static and dynamic responses of modular-block GRS-RWs. The details of the wall, including the modular blocks, geogrids, and soil are found in Liu (2002) or Ling et al. (2005a). For the present study, three different kinds of reinforcement layout were used: regular reinforcement layout having 10 layers of geogrids with length and spacing of 4.2 m (70% wall height) and 0.6 m (three blocks); short reinforcements having 10 layers of geogrids with length and spacing of 2.2 m (36.7% wall height) and 0.6 m, respectively; and large spacing reinforcements having six layers of geogrids with length and spacing of 4.2 m and 1.0 m, respectively. The geogrid reinforcements were assumed to be pinned to the facing blocks (i.e., an ideal connection between the facing blocks and the reinforcement layers). A 3-m foundation soil was considered in the analysis. The wall was 20-m deep into the backfill soil.

The backfill and foundation soils were modeled using a generalized plasticity model that simulates the pressure-dependent monotonic and cyclic behavior of sand (Ling and Liu 2003) and

the model parameters were the same as those used in the parametric study (Liu 2002), as shown in Table 2. The descriptions of the model and its capability in modeling the monotonic and cyclic behavior of sand could be found in Ling and Liu (2003) and thus it is not included herein. The behavior of the sandy backfill and foundation soils was assumed to be rate independent. The parameters for the HDPE geogrid (Ling et al. 1998) were used in the analyses, as summarized in Table 1. The parameters for the time-independent model can be found in Liu and Ling (2006). The FE mesh is shown in Fig. 10. Mesh sensitivities were analyzed for both static and seismic loadings. It was found that the FE mesh as shown in Fig. 10 is adequate for the simulation.

The construction behavior of the GRS retaining wall was first simulated using the construction simulation features of the FE program (Ling et al. 2004). For the time-independent analyses, the deformation and stress states after the completion of construction were used as the initial state for the seismic analysis. To simulate real earthquake behavior, the southwest and the vertical components of the 1995 Kobe earthquake [see Ling et al. (2005a)] were used as the excitation input at the base of the mesh. The maximum amplitude of the horizontal excitation was about 0.6 g while that for the vertical one was about 0.3 g. For the time-dependent analysis, the wall was allowed to creep for 3 years. The deformation and stress states at the end of construc-

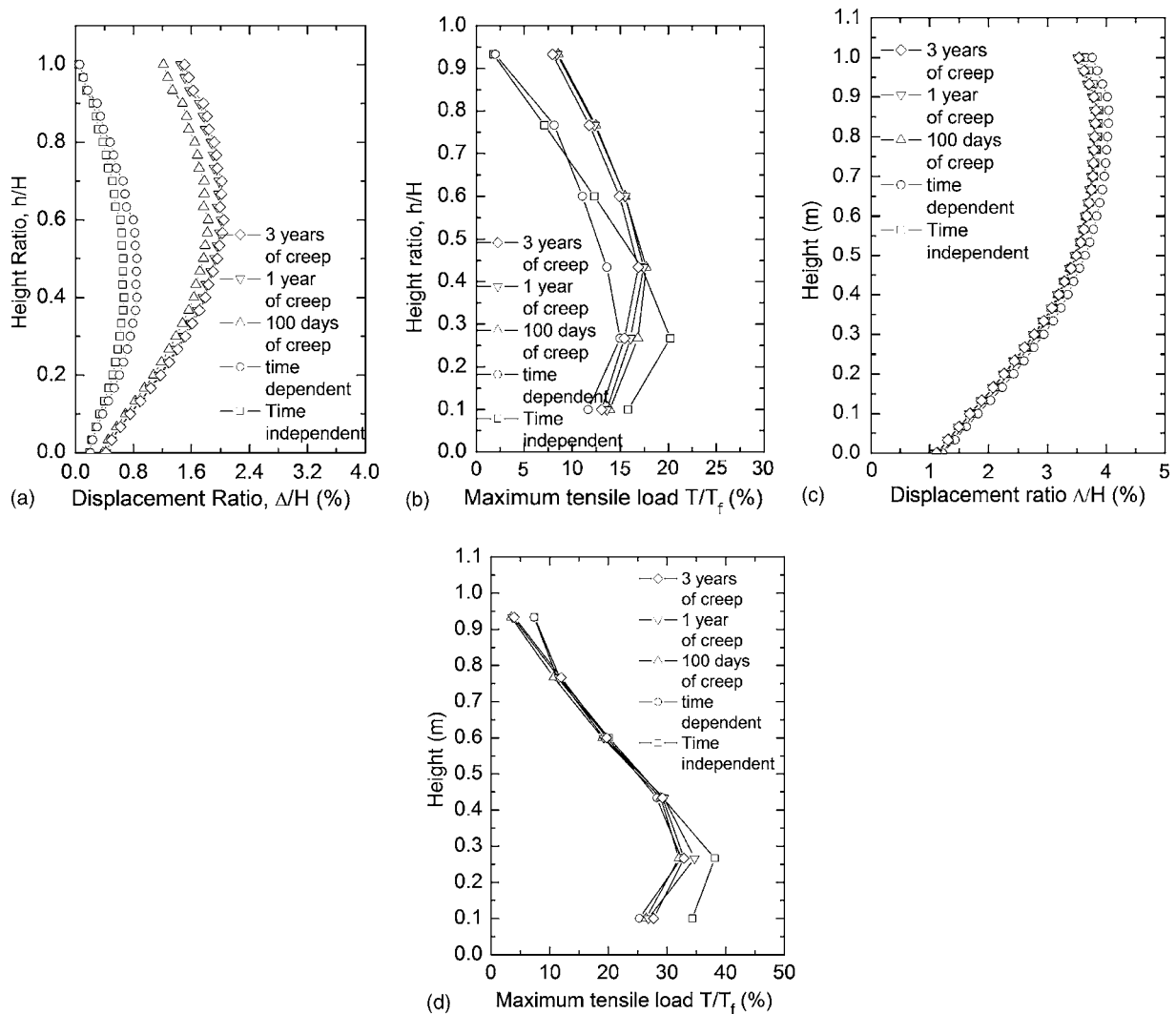


Fig. 14. Static and seismic performance of GRS-RW with large spacing reinforcements: (a) lateral displacement; (b) maximum load in the reinforcement layers; (c) lateral deformation of facing induced by earthquake; and (d) maximum reinforcement loads induced by earthquake

tion, and at 100 days, 1 year, and 3 years after construction were used as the initial state of the dynamic analyses, simulating the earthquake loading of the GRS-RW at different instants of service life. In the dynamic analyses, 5% of viscous system damping was included. A relatively large domain was considered in the analysis, with large size of elements and large damping properties (10% of viscous system damping) for the soil at the edge of the FE mesh in order to absorb possible reflection of vibration from the boundaries. The use of viscous damping in dynamic analysis of soil structures was discussed in Ling et al. (2005a).

Fig. 11 shows the results of the construction and creep analyses for the case with regular reinforcements. At the end of construction, the lateral displacement was not affected much by the time-dependent properties of the geosynthetic reinforcements [Fig. 11(a)]. However, the tensile load in the reinforcement layers was considerably affected. The maximum load in the reinforcement layers was small when the rate effect was considered [Fig. 11(b)], and the load distributions along the geogrid layers were also different. After creeping for a period of time, the lateral displacement of the wall increased, but the creep deformation ceased to develop after about one year. The time-dependent characteristics of the geosynthetics allowed further load redistribution in the reinforcement layers, as can be seen in Figs. 11(b and c).

Comparing the maximum loads in the reinforcements right after construction and those after a period of creep [Fig. 11(b), time-dependent model], it can be seen that the maximum loads increased and then decreased, indicating load redistributions in both the reinforcements and backfill soil during different periods of creep deformation of the wall.

The lateral displacements of the facing induced by earthquake loading are shown in Fig. 12(a). It can be seen that the maximum lateral displacements due to seismic loading occurred toward the top of the wall, which is consistent with the large-scale shakable test results reported by Ling et al. (2005b). The seismic-induced deformation of the GRS-RW was affected to some extent by the time-dependent properties of the reinforcement layers. The time-dependent properties of the geosynthetic reinforcements only affected the acceleration amplification (not given herein due to the scope of the paper) of the wall very slightly since the acceleration is predominantly affected by the soil properties (Ling et al. 2005a). The maximum loads in the reinforcement layers that are induced by the earthquake are shown in Fig. 12(b). The static loads are not included in Fig. 12(b). Similar to the lateral displacements, the reinforcement loads induced by the earthquake were slightly influenced by the time-dependent properties of the geogrids. The comparison of the maximum load distribution in-

Table 3. Differences in Lateral Deformations for Three Cases with Different Reinforcements

| | Differences in lateral deformation after completion with time-dependent and time-independent models (%H) | Differences in lateral deformation after 3-year creep with time-dependent and time-independent models (%H) |
|--|--|--|
| Regular reinforcements ($L=4.2$ m, $D=0.6$ m) | 0.087 | 0.75 |
| Short reinforcements ($L=2.2$ m, $D=0.6$ m) | 0.103 | 1.14 |
| Large spacing reinforcements ($L=4.2$ m, $D=1.0$ m) | 0.179 | 1.20 |

duced by the earthquake along the reinforcement layers is given in Fig. 12(c). A similar conclusion can be made regarding the load redistribution in the reinforcement layers.

The creep and seismic performance of the GRS-RW with short or large spacing reinforcements are given in Figs. 13 and 14, respectively. Similar conclusions can be obtained regarding the creep behavior for these two cases. At the end of construction, the lateral displacement was not considerably affected by the time-dependent properties of the geosynthetic reinforcements [Figs. 13(a) and 14(a)]. However, with short or large spacing reinforcements, the differences between the time-dependent and the time-independent results become larger, as shown in Table 3, especially for the case with large reinforcement spacing. The creep deformation of the GRS-RW also ceased to develop after about 1 year, but the creep deformation was larger with short or large spacing reinforcements, as shown in Table 3. The phenomena of load redistributions in the reinforcements are also similar to the case with regular reinforcement layout, as shown in Figs. 13(b) and 14(b). The earthquake-induced lateral deformations and maximum loads in the reinforcement layers are shown in Figs. 13(c and d) and 14(c and d) for these two cases. The magnitudes of the deformations and the maximum loads are larger than the case with regular reinforcement layout. Larger differences in the results can be seen between the time-dependent and time-independent cases.

The maximum lateral deformations of the GRS-RW with short or large spacing reinforcements after the earthquake excitation (with 3 years of creep) were about 6.5 and 5.8%H, respectively. Such large lateral deformations would prevent the GRS-RW from performing satisfactorily.

Conclusions and Discussions

A time-dependent constitutive model for geosynthetics was formulated based on bounding surface plasticity as well as viscoplasticity of Perzyna type. The model was used to predict the sophisticated cyclic and time-dependent behavior of different types of geosynthetics. The model was also developed in a hierarchical manner so that it can be used in the time-independent applications. The model was then incorporated into a finite-element code for analyzing GRS-RWs.

The following conclusions were obtained from this study:

1. Bounding surface plasticity and viscoplasticity of Perzyna type were relevant in simulating the time-dependent and cyclic behavior of geosynthetic materials, including rate dependency of stiffness, cyclic hysteresis, plastic strains under cyclic loading, creep, and load relaxation. The predictive capability of the model was validated against experimental results of different geosynthetics utilizing a single set of parameters.
2. The geosynthetic model allowed for sophisticated numerical analysis of GRS structures, from construction to sustained

creep/load relaxation, and seismic loadings during its service life. The lateral deformation of the GRS-RW at the end of construction was not greatly influenced by the time-dependent properties of geosynthetic reinforcements, but the loads in the reinforcements were considerably affected. The creep deformation of the wall developed after the end of construction, but it stabilized with time. The load redistribution in the reinforcement layers due to creep or load relaxation requires further consideration in the design of GRS-RWs.

3. The seismic behavior of the GRS retaining wall was also influenced to a certain extent by the time-dependent properties of the geosynthetic reinforcements, especially with short and large vertical spacing of reinforcements.
4. The effects of time-dependent properties of geosynthetics are more significant with short or large spacing reinforcement layouts, which affected creep deformation of GRS-RW.

The proposed model has to be calibrated with additional types of geosynthetics so that the parameters for different polymer types and density (mass per unit area) may be identified. Field full-scale tests would be most helpful in validating the analysis considering time-dependent behavior of geosynthetics. The creep of soils is not considered in the present study, which is adequate for granular backfill and foundations of GRS-RW. However, for soils with clayey contents, the creep effect could be quite significant, and the time-dependent properties of geosynthetic reinforcements could be more influential on the static and seismic performances of GRS structures. The creep behavior of GRS-RW after strong earthquake excitation may also be very important. These problems deserve further investigation.

Acknowledgments

This study was carried out with support from the National Science Foundation of China granted to the first writer (Grant No. 50408002). The support is gratefully acknowledged.

References

- Allen, T., Vinson, T. S., and Bell, J. R. (1982). "Tensile strength and creep behavior of geotextiles in cold regions applications." *Proc., 2nd Int. Conf. on Geotextiles*, Industrial Fabrics Association International, St. Paul, Minn., Vol. 2, 775–780.
- Andrewes, K. Z., McGown, A., and Murray, R. T. (1986). "The load-strain-time-temperature behavior of geotextiles and geogrids." *Proc., 3rd Int. Conf. on Geotextiles*, Industrial Fabrics Association International, St. Paul, Minn., Vol. 3, 707–712.
- Ashwamy, A. K., and Bourdeau, P. L. (1996). "Response of a woven and a non-woven geotextile to monotonic and cyclic simple tension." *Geosynth. Int.*, 3(4), 493–515.
- Bathurst, R. J., and Cai, Z. (1994). "In-isolation cyclic load-extension

- behavior of two geogrids." *Geosynthet. Int.*, 1(1), 1–19.
- Cai, Z., and Bathurst, R. J. (1995). "Seismic response analysis of geosynthetic-reinforced soil segmental walls by finite element method." *Comput. Geotech.*, 17(4), 523–546.
- Chan, A. H. C. (1993). *User manual for DYNA Swandye-II*, Dept. of Civil Engineering, Glasgow Univ., Glasgow, U.K.
- Dafalias, Y. F., and Popov, E. P. (1975). "A model of nonlinearly hardening materials for complex loading." *Acta Mech.*, 21(3), 173–192.
- Dafalias, Y. F., and Popov, E. P. (1976). "Plastic internal variables formalism of cyclic plasticity." *J. Appl. Mech.*, 98(4), 645–651.
- Dafalias, Y. F., and Popov, E. P. (1977). "Cyclic loading for materials with a vanishing elastic region." *Nucl. Eng. Des.*, 41(2), 293–302.
- Findley, W. N. (1987). "Twenty-six-year creep and recovery of poly (vinyl chloride) and polyethylene." *Polym. Eng. Sci.*, 27(8), 582–585.
- Finnigan, J. A. (1977). "The creep behavior of high tenacity yarns and fabrics used in civil engineering applications." *Proc., Int. Conf. on Use of Fabrics in Geotechnics*, Industrial Fabrics Association International, St. Paul, Minn., Vol. 2, 305–309.
- Gilat, A. (1984). "Modeling plastic deformation of mild steel under non-proportional deformation path." *J. Eng. Mater. Technol.*, 108(3), 258–261.
- Greenwood, J. H. (1990). "The creep of geotextiles." *Proc., 4th Int. Conf. on Geotextiles, Geomembranes, and Related Products*, Balkema, Rotterdam, The Netherlands, Vol. 2, 645–650.
- Helwany, B., and Wu, J. T. H. (1992). "A generalized creep model for geosynthetics." *Earth reinforcement practice*, Balkema, Rotterdam, The Netherlands, 79–84.
- Holtz, R. D., Tobin, W. R., and Burke, W. W. (1982). "Characteristics and stress-strain behavior of a geotextile-reinforced sand." *Proc., 2nd Int. Conf. on Geotextiles*, Industrial Fabrics Association International, St. Paul, Minn., Vol. 3, 805–810.
- Kaliakin, V. N., and Dafalias, Y. F. (1990a). "Theoretical aspects of the elastoplastic-viscoplastic bounding surface model for cohesive soils." *Soils Found.*, 30(3), 11–24.
- Kaliakin, V. N., and Dafalias, Y. F. (1990b). "Verification of the elastoplastic-viscoplastic bounding surface model for cohesive soils." *Soils Found.*, 30(3), 25–36.
- Kaliakin, V. N., and Dechasakulsom, M. (2002). "Development of a general time-dependent model for geogrids." *Geosynthet. Int.*, 9(4), 319–344.
- Koerner, R. M. (1997). *Design with geosynthetics*, 4th Ed., Prentice-Hall, Upper Saddle River, N.J.
- Krieg, R. D. (1975). "A practical two surface plasticity theory." *J. Appl. Mech.*, 47(3), 641–646.
- Kongkitkul, W., Hirakawa, D., Tatsuoka, F., and Uchimura, T. (2004). "Viscous deformation of geogrid reinforcement under cyclic loading conditions and its model simulation." *Geosynthet. Int.*, 11(2), 73–99.
- Leshchinsky, D., Dechasakulsom, M., Kaliakin, V. N., and Ling, H. I. (1997). "Creep and stress relaxation of geogrids." *Geosynthet. Int.*, 4(5), 463–479.
- Ling, H. I., and Liu, H. (2003). "Pressure-level dependency and densification behavior of sand through generalized plasticity model." *J. Eng. Mech.*, 129(8), 851–860.
- Ling, H. I., Liu, H., Kaliakin, V. N., and Leshchinsky, D. (2004). "Analyzing dynamic behavior of geosynthetic-reinforced soil retaining walls." *J. Eng. Mech.*, 130(8), 911–920.
- Ling, H. I., Liu, H., and Mohri, Y. (2005a). "Parametric studies on the behavior of reinforced soil retaining walls under earthquake loading." *J. Eng. Mech.*, 131(10), 1056–1065.
- Ling, H. I., Liu, H., Mohri, Y., and Kawabata, T. (2001). "Bounding surface model for geosynthetic reinforcements." *J. Eng. Mech.*, 127(9), 963–967.
- Ling, H. I., Mohri, Y., and Kawabata, T. (1998). "Tensile properties of geogrids under cyclic loadings." *J. Geotech. Geoenviron. Eng.*, 124(8), 782–787.
- Ling, H. I., Mohri, Y., Leshchinsky, D., Burke, C., Matsushima, K., and Liu, H. (2005b). "Large-scale shaking table tests on modular-block reinforced soil retaining walls." *J. Geotech. Geoenviron. Eng.*, 131(4), 465–476.
- Ling, H. I., Tatsuoka, F., and Tateyama, M. (1995). "Simulating performance of GRS-RW by finite-element procedure." *J. Geotech. Engrg.*, 121(4), 330–340.
- Liu, H. (2002). "Finite element simulation of the response of geosynthetic-reinforced soil retaining walls." Ph.D. thesis, Dept. of Civil Engineering and Engineering Mechanics, Columbia Univ., New York.
- Liu, H., and Ling, H. I. (2006). "Modeling cyclic behavior of geosynthetics using mathematical functions combined with Masing rule and bounding surface plasticity." *Geosynthet. Int.*, 13(6), 234–245.
- Lubliner, J. (1972). "On the thermodynamic foundations of nonlinear solid mechanics." *Int. J. Non-Linear Mech.*, 7(3), 237–254.
- Matichard, Y., Leclercq, B., and Sequin, M. (1990). "Creep of geotextiles: Soil reinforcement applications." *Proc., 4th Int. Conf. on Geotextiles, Geomembranes, and Related Products*, Balkema, Rotterdam, The Netherlands, Vol. 2, 661–665.
- Merry, S. M., and Bray, J. D. (1997). "Time-dependent mechanical response of HDPE geomembranes." *J. Geotech. Geoenviron. Eng.*, 123(1), 57–65.
- Moraci, N., and Montanelli, F. (1996). "Short and long term behavior of geogrids under static and cyclic load." *Earth reinforcement*, Balkema, Rotterdam, The Netherlands, 117–122.
- Pastor, M., Zienkiewicz, O. C., and Chan, A. H. C. (1990). "Generalized plasticity and the modeling of soil behavior." *Int. J. Numer. Analyt. Meth. Geomech.*, 14(3), 151–190.
- Perkins, S. W. (2000). "Constitutive modeling of geosynthetics." *Geotext. Geomembr.*, 18(5), 273–292.
- Perzyna, P. (1966). "Fundamental problems in viscoplasticity." *Adv. Appl. Mech.*, 9(3), 243–277.
- Petersson, H., and Popov, E. P. (1977). "Constitutive relations for generalized loadings." *J. Engrg. Mech. Div.*, 103(4), 611–627.
- Shen, C., Mamaghani, I. H. P., Mizuno, E., and Usami, T. (1995). "Cyclic behavior of structural steels. II: Theory." *J. Eng. Mech.*, 121(11), 1165–1172.
- Shrestha, S. C., and Bell, J. R. (1982). "Creep behavior of geotextiles under sustained loads." *Proc., 2nd Int. Conf. on Geotextiles*, Industrial Fabrics Association International, St. Paul, Minn., Vol. 3, 769–774.
- Soong, T. Y., and Koerner, R. M. (1998). "Modeling and extrapolation of creep behavior of geosynthetics." *Proc., 6th Int. Conf. on Geotextiles*, Industrial Fabrics Association International, St. Paul, Minn., Vol. 2, 769–774.
- Tanimoto, N., Fukuoka, H., and Fujita, K. (1993). "One-dimensional numerical analysis of a bar subjected to longitudinal impulsive loading using an elastoplastic-viscoplastic constitutive equation." *JSME Int. J., Ser. A*, 36(2), 137–145.
- Wu, J. T. H., and Helwany, S. M. N. (1996). "A performance test for assessment of long-term creep behavior of soil geosynthetic composites." *Geosynthet. Int.*, 3(1), 107–124.